Received: 18 June 2020 | Revised: 10 November 2020 | Accepted: 14 December 2020

IET Microwaves, Antennas & Propagation

DOI: 10.1049/mia2.12091

The Institution of Engineering and Technology WILEY

ORIGINAL RESEARCH PAPER

Optimisation-based design of transversal signal-interference microwave bandpass and lowpass filters with extended stopband

Roberto Gómez-García | **Li Yang** | **José-María Muñoz-Ferreras**

Department of Signal Theory & Communications, University of Alcalá, Alcalá de Henares, Madrid, Spain

Correspondence

Roberto Gómez-García, Department of Signal Theory and Communications, University of Alcalá, Alcalá de Henares, Madrid, Spain.
Email: roberto.gomez.garcia@ieee.org

Funding information

Spanish Ministry of Economy, Industry, and Competitiveness (State Research Agency), Grant/Award Number: TEC2017-82398-R; H2020-MSCA-COFUND programme GOT ENERGY TALENT, Grant/Award Number: 754382

Abstract

Generalised bi-path stepped-impedance-line signal-interference bandpass and lowpass transversal filtering sections (TFSs) with increased stopband bandwidth above the main transmission band are presented. They are realised by partitioning the two in-parallel transmission-line paths in their related classic spectrally periodic TFS approach into a plurality of line sub-segments, whose characteristic-impedance and electrical-length values are derived through optimisation. It is demonstrated that the stopband range above the transmission band in these generalised non-frequency-periodic TFSs can be remarkably broadened with regard to those intrinsic to their conventional bandpass and lowpass TFS counterparts. Furthermore, as added benefits, this is achieved for shorter transmission-line paths and a sharper cut-off slope between the transmission band and the extended stopband. For experimental-validation purposes, three proof-of-concept microstrip prototypes are manufactured and characterised. They correspond to a 1-GHz bandpass TFS, a 1-GHz two-TFS-in-series-cascade-based bandpass filter (BPF) with augmented selectivity and out-of-band power-rejection levels, and one lowpass TFS with a designed 3-dB cut-off frequency of 1.25 GHz.

1 | INTRODUCTION

In the last few years, signal-interference RF/microwave passive bandpass filters (BPFs) have become a suitable alternative to coupled-resonator-based BPF networks. Owing to their intrinsic capability to generate transmission bands and out-of-band power transmission zeroes (TZs) by means of constructive and destructive transversal signal-energy interactions, respectively, they allow to perform quasi-elliptic-type filtering actions with sharp-rejection capabilities. Their constituent stages, commonly referred to as 'transversal filtering sections' (TFSs), are multi-path circuit structures in which the feedforward signal-interference phenomenon takes place at their output nodes once the input-signal components have propagated through their electrical paths. The most basic example of TFS is the one consisting of two in-parallel transmission-line segments, which has been applied to single- and multi-band BPF design even with reflectionless and flattened-passband features [1–4]. Other examples of TFSs available in the technical literature exploit directional power couplers for static- and switchable-bandwidth BPF development, coupled-line sections for ultra-wideband BPF designs, baluns, left-handed cells for more-compact BPF realisations, modified schemes with stubs to incorporate notches within the BPF wide-passband range, and even hybridised acoustic-wave-resonator/transmission-line circuit topologies for narrower-band BPFs [5–11]. Other examples of filtering functionalities addressed by the transversal signal-interference philosophy are the bandstop type and its application in high-selectivity lowpass-filter (LPF) design with both fixed and controllable cut-off frequency [12–14], as well as the implementation of frequency-static quasi-elliptic-type highpass-filtering devices [15].

It must be remarked upon that most of the aforementioned transversal signal-interference BPFs are shaped by transmission-line sections whose electrical lengths are multiples of 90° at the passband centre frequency. As a result, the obtained bandpass filtering transfer functions are frequency periodic, which results in relatively narrow upper-stopband bandwidths [16]. This could limit their usefulness in a number of practical applications, where very-broad upper-stopband ranges are required to efficiently mitigate the interfering RF signals above

the main transmission band. The same shortcoming is found in bandstop-TFS-based LPFs, where several stages with spectrally-adjacent stopbands need to be cascaded in series to further enlarge the attenuated band, but at the expense of a significantly-increased circuit size [14, 17].

A new class of generalised bandpass and lowpass TFSs with stepped-impedance transmission-line paths is reported here. Although a preliminary TFS approach using stepped-impedance lines was proposed in [18] to introduce spectral asymmetry in dual-band BPFs and channelising BPFs for diplexers, the extension of the upper-stopband bandwidth was not addressed as the design goal. Therefore, this work complements the previous study by overcoming one of the main limitations of most of signal-interference bandpass TFSs, known as their narrow upper stopbands, and by extending this concept to broadened-attenuated-band lowpass TFSs. In the case of BPFs, unlike the approach in [19] that combines bandpass TFSs with a type of modified input/output interdigital feeding sections to extend the upper-stopband bandwidth, no coupling sections are required here. On the other hand, when compared to in-series-cascaded bandstop-TFS-based LPF solutions as in [14], a single generalised lowpass TFS is capable of featuring the extended-stopband characteristics by itself. Furthermore, this work demonstrates for the first time on how stepped-impedance-transmission-line principles, which have been extensively exploited over the years in coupled-resonator microwave planar and non-planar BPF topologies to further enlarge the upper-stopband bandwidth by pushing the spurious bands to higher frequencies (e.g., see [20–22]), can also be applied to signal-interference BPFs for the same goal, although, from a different operational perspective. The rest of the manuscript is organised as follows. The optimisation-based designs of two different examples of generalised bandpass TFSs and one example of generalised lowpass TFS with extended stopband above the main transmission band are presented in Section 2. Furthermore, in Section 3, three proof-of-concept microstrip prototypes that correspond to a bandpass TFS, a two-TFS-based BPF, and a lowpass TFS are designed, manufactured, and characterised for experimental-demonstration purposes. Finally, a summary and the most relevant concluding remarks of this work are provided in Section 4.

2 | GENERALISED STEPPED-IMPEDANCE-LINE TFSs

2.1 | Bandpass TFS

The circuit detail of the engineered bi-path generalised signal-interference bandpass TFS is shown in Figure 1. As seen in the figure, it is shaped by the in-parallel connection of two transmission-line-based paths. Nevertheless, when compared with its traditional bandpass TFS counterpart in [1] that is composed of two in-parallel uniform-impedance transmission-line segments, each of these electrical paths here is divided into a plurality of in-series-cascaded line sub-segments with

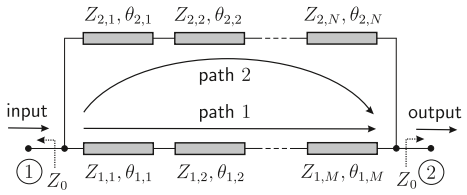

FIGURE 1 Circuit detail of the proposed generalised signal-interference bandpass TFS (Z_0 is the reference impedance)

different characteristic impedances and electrical lengths. In this manner, a generalised stepped-impedance-line bandpass TFS is obtained. In particular, M and N line sub-segments are considered in the transmission-line paths 1 and 2 in the TFS depicted in Figure 1, whereas Z and θ variables refer to characteristic impedances and electrical lengths, respectively.

The main purpose of using stepped-impedance lines in the two electrical paths of the proposed TFS design is to mitigate the spectral periodicity inherent to its related conventional TFS approach in [1]. Indeed, this classic TFS was applied to the realisation of wide-band bandpass filtering transfer functions with spectral symmetry with regard to its centre frequency f_0 by means of constructive/destructive signal-interference phenomena. For this aim, the electrical lengths of its uniform-impedance transversal paths are selected as multiples of 90° at f_0 by following specific analytically-derived design equations for them and the line impedances [1]. Nevertheless, this leads to a frequency-periodic filtering transfer function with period $2f_0$, so that a narrow upper stopband is realised in the first spectral period $[0, 2f_0)$ owing to the appearance of additional upper transmission bands. Moreover, higher the difference between the electrical lengths of the two uniform-impedance transmission-line paths, narrower the bandwidths of the main passband and the upper stopband. Hence, by generalising each transmission-line path as the in-series cascade of multiple different-length/impedance line sub-segments, the signal-cancellation effect above the main passband can be further extended to create a very-enlarged upper stopband. In this manner, an improved version of the classic bandpass TFS is obtained with a much-broader upper-stopband bandwidth and is no longer frequency periodic.

Due to the mathematical difficulty involved in the analytical design of this generalised bandpass TFS, an optimisation-based approach is selected to illustrate the suggested filter concept. Such a design procedure, whose flowchart is illustrated in Figure 2, consists of the following steps:

- **Step 1.** Design of a classic ideal bandpass TFS by means of [1] to meet a prefixed specification in terms of passband width (i.e., minimum input/output power-matching level $\Gamma_{\min}$ within a certain in-band frequency range (f_{c1}, f_{c2})). The values of the characteristic impedances and electrical lengths of the two uniform-impedance transmission-line paths of this basic TFS are designated as Z_1, Z_2 and θ_1, θ_2 $(\theta_2 > \theta_1)$, respectively. Besides, $L_{\text{rej}}^{\min}$ is the minimum power-rejection level of the resulting lower and upper stopbands in this basic TFS.

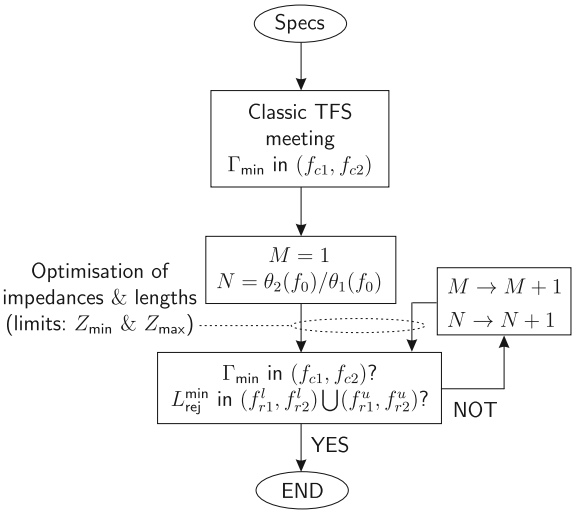

FIGURE 2 Flowchart of the optimisation-based design algorithm

- **Step 2.** Division of the two transmission-line paths 1 and 2 of the classic bandpass TFS derived from Step 1 into M and N line sub-segments, respectively, where their characteristic impedances and electrical lengths at f_0 correspond to the design variables that have to be optimised. As the starting point, all these line sub-segments are assumed to have the same line-impedance value as the associated path in the classic bandpass TFS and identical length (i.e., $Z_{1,i} = Z_1$, $Z_{2,j} = Z_2$, $\theta_{1,i} = \theta_1/M$, and $\theta_{2,j} = \theta_2/N$ where $i = 1, 2, \ldots, M$ and $j = 1, 2, \ldots, N$). Moreover, in the first iteration and as the initial choice, only the longest transmission-line path is partitioned into a number of line sub-segments whose lengths are equal to the one of the shortest transmission-line path (i.e., $M = 1$ and $N = \theta_2(f_0)/\theta_1(f_0)$ in the first iteration).
- **Step 3.** Optimisation of the design variables through conventional optimisation techniques (e.g., ordinary least-squares or gradient-based methods that are available in commercial circuit-simulation tools) in order to extend the upper-stopband bandwidth to at least the desired spectral interval (f_{r1}^u, f_{r2}^u) for a minimum stopband-power-rejection level L_{rej}^{min}, while keeping Γ_{min} within (f_{c1}, f_{c2}) and L_{rej}^{min} for at least a lower-stopband interval (f_{r1}^l, f_{r2}^l) equal to that of the classic TFS derived from Step 1. The minimum and maximum permissible line-impedance values are set as Z_{min} and Z_{max}, respectively.
- **Step 4.** If Step 3 cannot be accomplished (i.e., the cost function of the selected optimisation method as mentioned in Step 3 does not tend to zero after several iterations and it does not converge), return to Step 2 by considering a higher number of line sub-segments in each transmission-line path (i.e., increase M and N).

The previous optimisation-based design technique has been applied to two different ideal bandpass TFS design examples referred here as 'example 1' and 'example 2'. The values for the design variables and main spectral characteristics obtained for the related classic bandpass TFSs derived through Step 1 for both examples are listed below:

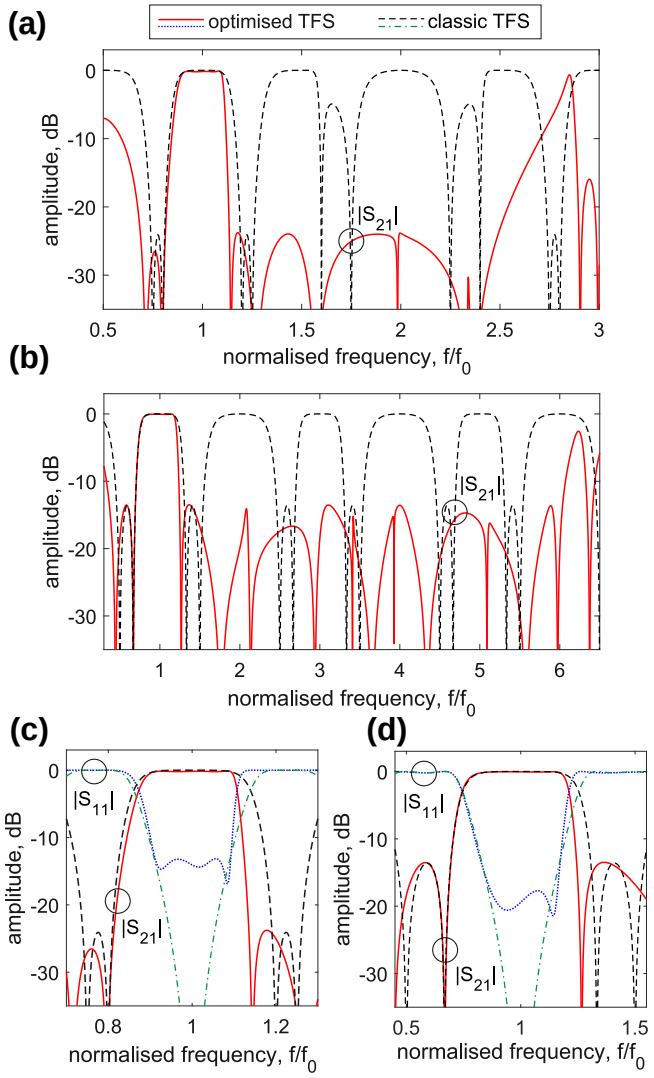

FIGURE 3 Theoretical power transmission ($|S_{21}|$) and reflection ($|S_{11}|$) responses of the optimised and classic bandpass TFSs for example 1 and 2

a Example 1: $|S_{21}|$ (broad-band response)
b Example 2: $|S_{21}|$ (broad-band response)
c Example 1: $|S_{21}|$ and $|S_{11}|$ (transmission-band detail)
d Example 2: $|S_{21}|$ and $|S_{11}|$ (transmission-band detail)

- **Example 1.** $Z_1 = Z_2 = 2Z_0$, $\theta_1(f_0) = 90°$, $\theta_2(f_0) = 810°$, $\Gamma_{min} = 13$ dB within $(f_{c1}, f_{c2}) \equiv (0.91f_0, 1.09f_0)$, and $L_{rej}^{min} = 23.5$ dB within lower- and upper-stopband frequency ranges of $(f_{r1}^l, f_{r2}^l) \equiv (0.74f_0, 0.81f_0)$ and $(f_{r1}^u, f_{r2}^u) \equiv (1.19f_0, 1.26f_0)$, respectively.
- **Example 2.** $Z_1 = Z_2 = 2Z_0$, $\theta_1(f_0) = 90°$, $\theta_2(f_0) = 450°$, $\Gamma_{min} = 15$ dB within $(f_{c1}, f_{c2}) \equiv (0.84f_0, 1.16f_0)$, and $L_{rej}^{min} = 13.5$ dB within lower- and upper-stopband frequency ranges of $(f_{r1}^l, f_{r2}^l) \equiv (0.46f_0, 0.69f_0)$ and $(f_{r1}^u, f_{r2}^u) \equiv (1.31f_0, 1.54f_0)$, respectively.

The power transmission and reflection responses of the classic bandpass TFS and the generalised bandpass TFS in Figure 1 derived with the proposed optimisation-based design

TABLE 1 Design variables of the optimised bandpass TFSs for example one and two

Example 1 ($M = 1$, $N = 22$, $Z_{1,1} = 3.1Z_0$, $\theta_{1,1}(f_0) = 48.3°$)					
j	$Z_{2,j}/Z_0$	$\theta_{2,j}(f_0)$	j	$Z_{2,j}/Z_0$	$\theta_{2,j}(f_0)$
1	0.74	11.2°	12	2	12.5°
2	0.4	48.5°	13	0.61	45°
3	1.054	17.5°	14	3.1	50.3°
4	0.94	21°	15	1.28	50.5°
5	0.404	49.8°	16	2	26.4°
6	3.1	50.2°	17	3.1	33°
7	2	7.4°	18	0.932	50.3°
8	3.1	31.9°	19	3.1	41.5°
9	1.2	34.2°	20	1.15	32°
10	2.254	34.6°	21	1.7	40.3°
11	2	6.4°	22	0.65	38°
Example 2 ($M = 1$, $N = 12$, $Z_{1,1} = 3.1Z_0$, $\theta_{1,1}(f_0) = 48.8°$)					
j	$Z_{2,j}/Z_0$	$\theta_{2,j}(f_0)$	j	$Z_{2,j}/Z_0$	$\theta_{2,j}(f_0)$
1	0.422	25.7°	7	1	22.6°
2	3.1	6.4°	8	0.38	50°
3	3.1	5.6°	9	3.1	19.7°
4	1.156	13.4°	10	0.854	60.2°
5	0.462	53.5°	11	3.1	40.3°
6	0.404	43.5°	12	0.956	50°

procedure for examples 1 (Figure 3*a* and *c*) and 2 (Figure 3*b* and *d*) are compared in Figure 3. The values for the design variables of the optimised bandpass TFSs are listed in Table 1 ($Z_{\min} = 0.36Z_0$ and $Z_{\max} = 3.1Z_0$ were chosen), where it is found that the shortest path tends to a uniform-impedance transmission-line segment with $Z_{\max}$ line impedance for both examples. Please note that, due to the high mathematical complexity involved in the theoretical analysis of the generalised TFS scheme in Figure 1, no closed rules to select the optimum values for M and N from the prefixed specifications to be met can be established. Moreover, as seen in Table 1, $M = 1$ for both examples after joining into one all the line sub-segments of path one, which tend to reach the same value for their characteristic impedances at the end of the optimisation algorithm. As shown in Figure 3, the proposed approach is successful in considerably enlarging the upper-stopband bandwidths with regard to those of the classic TFS designs through the reallocation of the TZs (i.e., fully-destructive signal-interference combinations between paths) to suppress the upper transmission bands. Specifically, upper-stopband ranges of $(f^u_{r1}, f^u_{r2}) = (1.14f_0, 2.49f_0)$ and $(f^u_{r1}, f^u_{r2}) = (1.25f_0, 6.03f_0)$

For example one and two are obtained, respectively, which are 19.3 and 20.8 times larger than those resulting for the

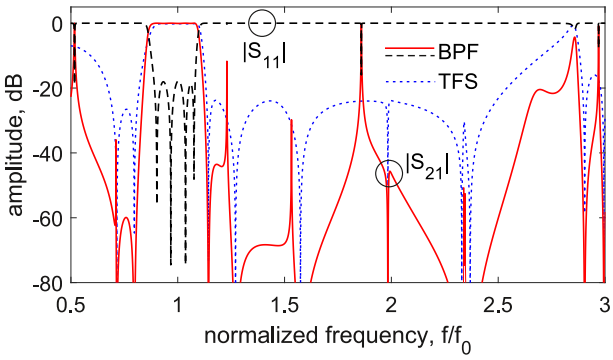

FIGURE 4 Theoretical power transmission ($|S_{21}|$) and reflection ($|S_{11}|$) responses of the two-TFS-based BPF and $|S_{21}|$ of its constituent TFS

classic TFSs with homogeneous-characteristic-impedance transmission-line paths. This is carried out while keeping the in-band power-matching and lower-stopband-attenuation requisites in the optimised TFSs, and while shortening the total electrical lengths for both transversal transmission-line paths (in particular, 48.3° and 732.5° vs. 90° and 810° at f_0 e.g. 1 and 48.8° and 390.9° vs. 90° and 450° at f_0 e.g. 2, respectively) and making sharper the cut-off slope in the upper-passband region.

a Example 1: $|S_{21}|$ (broad-band response)
b Example 2: $|S_{21}|$ (broad-band response)
c Example 1: $|S_{21}|$ and $|S_{11}|$ (transmission-band detail)
d Example 2: $|S_{21}|$ and $|S_{11}|$ (transmission-band detail)

Finally, it should be remarked upon that multi-TFS in-series-cascade-based BPF architectures can be designed for the realisation of higher stopband-rejection and selectivity levels. For illustration purposes, Figure 4 shows the power transmission and reflection responses of a two-TFS-based BPF design based on the mirrored in-series cascade connection of two replicas of the generalised bandpass TFS in example 1. An inter-TFS cascading line with characteristic impedance $Z_c = 1.6Z_0$ and $\theta_c(f_0) = 18.5°$ was employed, whereas input/output transmission-line sections with characteristic impedance $Z_m = 2.12Z_0$ and $\theta_m(f_0) = 182°$ were used for in-band power-matching purposes. As proven, when compared with the transfer function of its building bandpass TFS, both the selectivity and out-of-band power attenuation levels are considerably increased. Also note that the presence of the out-of-band spikes is due to the cascading process, as discussed in [23], and they appear at the spectral positions $\{f_p\}$ that satisfy $\theta(f_p) = \phi_{22}^{Z_c}(f_p) + k\pi$ ($k \in \mathbb{Z}$ and $\phi_{22}^{Z_c}$ is the phase of the S_{22} parameter of the TFS referred to Z_c). Hence, in order to avoid the generation of a spike at some specific frequency locations f_p, the previous equation can be added as a constraint in the optimisation-based inter-TFS-cascade design process so that such a condition is not fulfiled at f_p.

2.2 | Lowpass TFS

As demonstrated in [12], by properly selecting the electrical lengths of the transmission-line segments of the classic TFS reported in [1], a bandstop-type filtering action centred at f_0

with signal transmission below this band (i.e., lowpass-type filtering functionality hereafter) can be attained. This is achieved by producing a destructive inter-path signal-energy cancellation at f_0 instead of a constructive one as in the bandpass TFS version. Although the stopband bandwidth can be increased by tuning the characteristic-impedance variables of the lowpass TFS for fixed electrical lengths, this can be carried out to certain extent. Larger stopband bandwidths for extended-stopband LPF design are feasible by in-series cascading various lowpass TFSs with spectrally-adjacent stopbands, which leads to an increased circuit size. However, by using the same optimisation-based design technique as in Section 2.1, generalised stepped-impedance-line lowpass TFSs, as in Figure 1, that exhibit the enlarged-stopband property by themselves can be designed.

The optimisation-based design method described in Section 2.1 (but adapted to a lowpass-type transfer function) has been applied to an ideal lowpass TFS design example, referred to as 'example 3'. The values for the design parameters and the main frequency characteristics of the associated conventional lowpass TFS obtained from Step 1 are as follows:

- **Example 3.** $Z_1 = 3.1Z_0$, $Z_2 = 2Z_0$, $\theta_1(f_0) = 180°$, $\theta_2(f_0) = 360°$, minimum input/output power-matching level of $\Gamma_{min} = 15$ dB from 0 to $f_c = 0.461f_0$, and $L_{rej}^{min} = 19.7$ dB within the stopband frequency range of $(f_{r1}, f_{r2}) \equiv (0.742f_0, 1.258f_0)$.

The power transmission and reflection responses of the conventional lowpass TFS and the generalised lowpass TFS ,as in Figure 1 ,derived with the proposed optimisation-based design technique are compared in Figure 5. The values for the design variables of the optimised lowpass TFS are indicated in Table 2 ($Z_{min} = 0.36Z_0$ and $Z_{max} = 3.1Z_0$ were selected). In particular, the optimised lowpass TFS features a 19.7-dB-referred stopband bandwidth $(f_{r1}, f_{r2}) \equiv (0.755f_0, 3.014f_0)$ (i.e., 4.4 times larger than that of the classic lowpass TFS with uniform-characteristic-impedance transmission-line paths) while maintaining the input-power-matching specification in the transmission band. Furthermore, this is again achieved for shorter length transmission-line paths in the generalised lowpass TFS (in particular, 48.8° and 299.1° vs. 90° and 360° at f_0, respectively) and a lowpass-filtering transfer function with sharper transmission-band-to-stopband transition as simultaneous benefits.

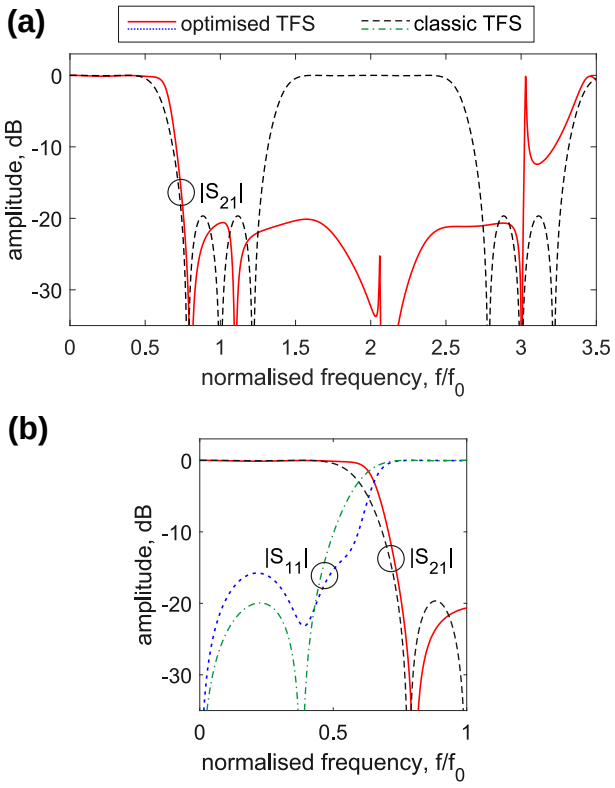

FIGURE 5 Theoretical power transmission ($|S_{21}|$) and reflection ($|S_{11}|$) responses of the optimised and classic lowpass TFSs for example three
a $|S_{21}|$ *(broad-band response)*
b $|S_{21}|$ *and* $|S_{11}|$ *(transmission-band detail)*

TABLE 2 Design variables of the optimised lowpass TFS for example three

Example 3 ($M = 1$, $N = 12$, $Z_{1,1} = 3.1Z_0$, $\theta_{1,1}(f_0) = 176.5°$)					
j	$Z_{2,j}/Z_0$	$\theta_{2,j}(f_0)$	j	$Z_{2,j}/Z_0$	$\theta_{2,j}(f_0)$
1	0.82	48.9°	7	2.38	6.6°
2	0.9	43.4°	8	0.4	34.6°
3	2.34	31.1°	9	2.7	7.5°
4	2.44	17.3°	10	2.4	7.8°
5	2.4	22°	11	3.1	34.8°
6	2.4	10.9°	12	0.42	34.2°

3 | EXPERIMENTAL RESULTS

3.1 | Bandpass prototypes

To demonstrate the practical feasibility of the proposed approach of generalised signal-interference bandpass TFS with extended upper stopband, two 1-GHz microstrip bandpass prototypes ($Z_0 = 50$ Ω) have been developed and characterised. They correspond to the optimised bandpass TFS in example 1 (Figure 3*a* and *c*), and a BPF based on the mirrored in-series cascade of two replicas of this TFS (Figure 4). For their fabrication, a Rogers 4003C substrate with the following parameters was employed: relative dielectric permittivity $\varepsilon_r = 3.38$, dielectric thickness $H = 1.524$ mm, metal thickness $t = 17.8$ μm, and dielectric loss tangent $\tan(\delta_D) = 0.0027$. The simulation and optimisation processes of these bandpass prototypes were performed with the electromagnetic-(EM)-software package Ansys HFSS, whereas their measurements in terms of *S*-parameters were taken by means of an Agilent E8361A vector network analyser.

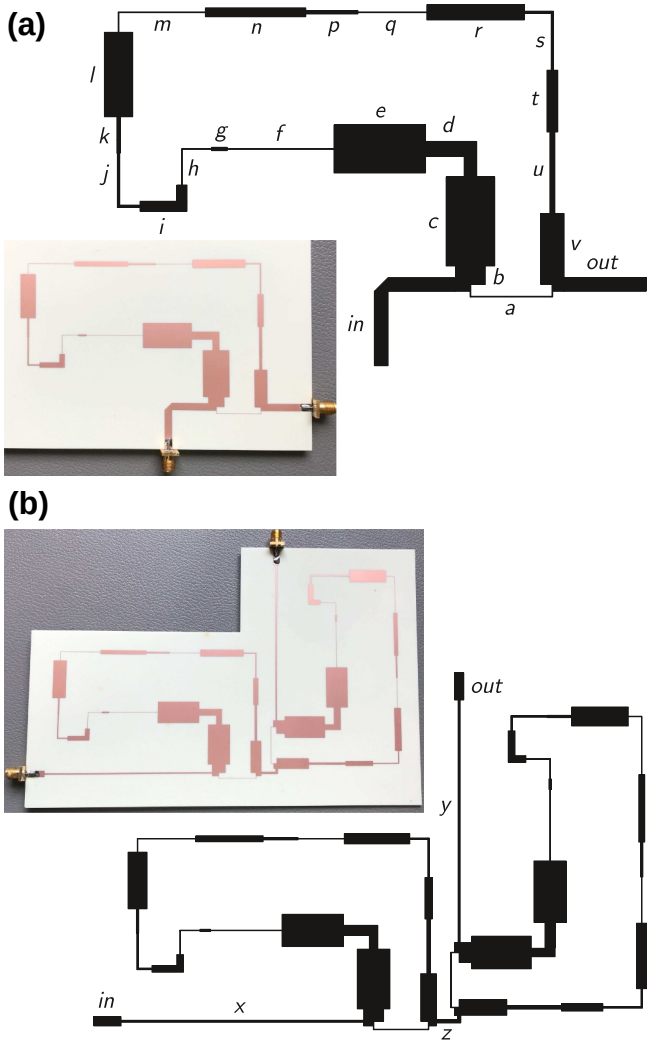

FIGURE 6 Layouts and photographs of the manufactured microstrip bandpass prototypes

a) *TFS (non-redundant dimensions, in mm ['w' stands for widths and 'l' for middle lengths including bends when applicable, but not considering T-junction regions]:* $w_{in} = w_{out} = 3.38$, $l_{in} = 37.22$, $l_{out} = 20.2$, $w_a = 0.172$, $l_a = 22.61$, $w_b = 7.32$, $l_b = 2.87$, $w_c = 11.96$, $l_c = 21.92$, $w_d = 3.71$, $l_d = 14.55$, $w_e = 11.82$, $l_e = 22.54$, $w_f = 0.172$, $l_f = 26.26$, $w_g = 0.81$, $l_g = 3.88$, $w_h = 0.172$, $l_h = 16.17$, $w_i = 2.47$, $l_i = 15.56$, $w_j = 0.58$, $l_j = 18.34$, $w_k = 0.81$, $l_k = 9$, $w_l = 6.96$, $l_l = 20.78$, $w_m = 0.172$, $l_m = 26.32$, $w_n = 2.19$, $l_n = 24.72$, $w_p = 0.81$, $l_p = 12.84$, $w_q = 0.172$, $l_q = 16.96$, $w_r = 3.76$, $l_r = 24.02$, $w_s = 0.54$, $l_s = 21.16$, $w_t = 2.66$, $l_t = 15.2$, $w_u = 1.22$, $l_u = 20.08$, $w_v = 5.78$, and $l_v = 15.79$).

b) *Two-TFS-based BPF* (non-redundant dimensions, in mm ['w' stands for widths and 'l' for middle lengths including bends when applicable but not considering T-junction regions]: $w_{in} = w_{out} = 3.38$, $l_{in} = l_{out} = 10$, $w_x = w_y = 0.73$, $l_x = l_y = 89.05$, $w_z = 1.2$, and $l_z = 10.55$; the dimensions of the building TFS are the same as in Figure 6*a* except for the corresponding modifications of the widths in those line segments connected to the T-junctions).

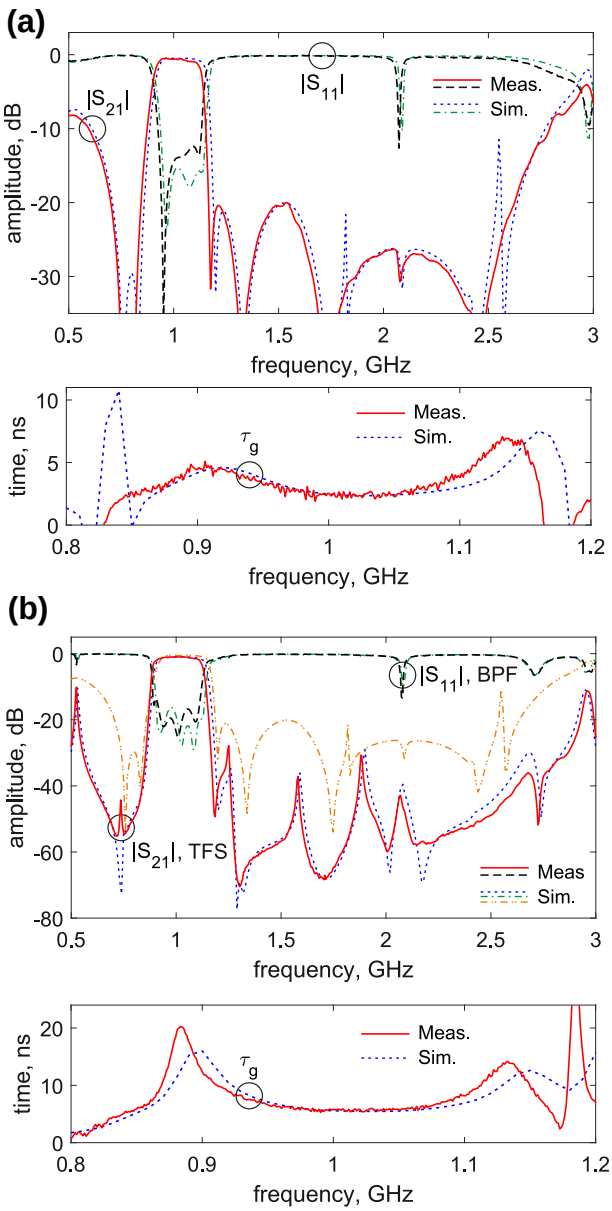

FIGURE 7 Simulated and measured power transmission ($|S_{21}|$), reflection ($|S_{11}|$), and in-band group-delay (τ_g) responses of the manufactured microstrip bandpass prototypes

a TFS.

b Two-TFS-based BPF and TFS (simulated $|S_{21}|$)

The layouts and photographs of the developed bandpass prototypes with indication of their main dimensions are shown in Figure 6. Their simulated and measured power transmission, reflection, and in-band group-delay responses are compared in Figure 7. As it can be seen, a fairly-close agreement between measurements and simulations is obtained. The main performance metrics of the developed prototypes of bandpass TFS and two-TFS-based BPF, respectively are measured as follows: centre frequencies of 1.02 and 1 GHz, 3-dB absolute bandwidths of 235 and 237 MHz (i.e., equal to 23% and 23.7% in relative terms), minimum in-band power-insertion-loss levels of 0.48 and 0.87 dB, minimum in-band input-power-matching levels equal to 12.4 and 13.4 dB, and maximum in-band group-delay variations of 4.4 and 14.6 ns. The bandpass TFS features a measured 20-dB-attenuation-referred extended upper stopband in the range 1.166–2.625 GHz, whereas the two-TFS-based BPF show considerably-augmented power-rejection levels in most of the aforementioned stopband

interval (i.e., apart from the presence of some undesired narrow-band out-of-band spurious spikes in the two-TFS-based BPF prototype, as mentioned in Section 2.1) as a result of the two-TFS in-series-cascading process.

3.2 | Lowpass prototype

A microstrip proof-of-concept prototype of the generalised signal-interference lowpass TFS example in Figure 5 with an extended stopband ($Z_0 = 50\ \Omega$) has also been constructed and measured for experimental-validation purposes. A 3-dB cut-off frequency of 1.25 GHz was selected for this circuit, and the same logistic media and substrate as in the previous prototypes were employed for its simulation, fabrication, and measurement processes.

The layout and photograph of the manufactured lowpass prototype with indication of its basic dimensions are provided in Figure 8, whereas its simulated and measured power transmission, reflection, and in-band group-delay responses are represented in Figure 9. Again, the agreement obtained between simulations and measurements is close enough to verify the proposed filter design principle. The main measured characteristics of this lowpass TFS prototype are as follows: 3-dB cut-off frequency of 1.264 GHz, minimum in-band input-power-matching level equal to 15.3 dB, upper stopband in the interval 1.478–5.837 GHz referred to a power-attenuation level of 20.6 dB, and maximum in-band group-delay variation equal to 1 ns.

4 | CONCLUSION

A new family of bi-path signal-interference lowpass and bandpass TFSs with enlarged attenuated band above the main transmission band has been proposed. These novel TFSs consist of two in-parallel transmission-line paths, which are divided into multiple line sub-segments with different characteristic impedances and electrical lengths. The values of their design parameters are optimised to enlarge the referred stopband in the generalised TFS approach by breaking the spectral periodicity inherent to its conventional TFS counterpart. Two theoretical design examples for a bandpass TFS and one example for a lowpass TFS have been provided to validate this filter design principle. Moreover, for experimental-verification purposes, two 1-GHz microstrip bandpass prototypes based on a single TFS and on the mirrored cascade of two replicas of this TFS and one microstrip lowpass TFS circuit with a designed 3-dB cut-off frequency of 1.25 GHz have been developed and measured. In addition to featuring a much-broader stopband bandwidth above the main transmission band, further advantages of these generalised stepped-impedance-line TFSs when compared with their related traditional TFS schemes are shorter transmission-line paths and

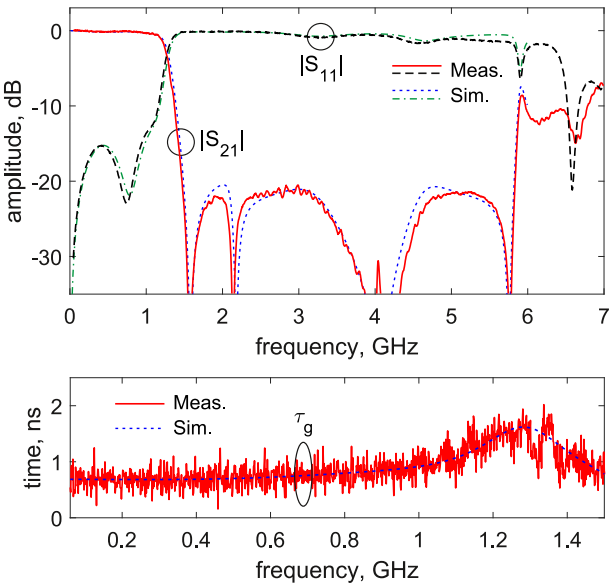

FIGURE 9 Simulated and measured power transmission ($|S_{21}|$), reflection ($|S_{11}|$), and in-band group-delay (τ_g) responses of the manufactured microstrip lowpass TFS prototype

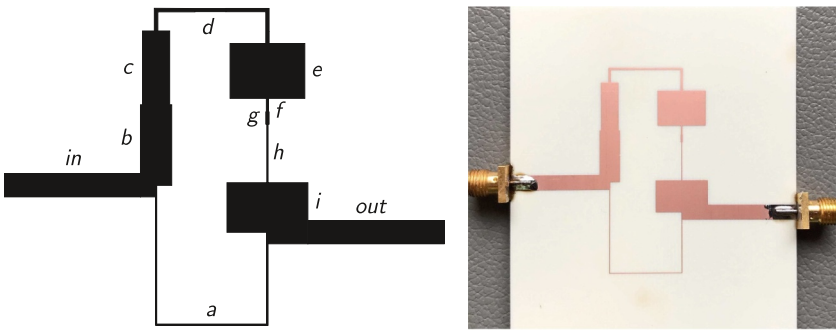

FIGURE 8 Layout and photograph of the manufactured microstrip lowpass TFS prototype (non-redundant dimensions, in mm ['w' stands for widths and 'l' for middle lengths including bends when applicable but not considering T-junction regions]: $w_{in} = w_{out} = 3.38$, $l_{in} = l_{out} = 20$, $w_a = 0.172$, $l_a = 46.96$, $w_b = 4.58$, $l_b = 10.12$, $w_c = 3.98$, $l_c = 10.83$, $w_d = 0.511$, $l_d = 24.35$, $w_e = 10.96$, $l_e = 8.04$, $w_f = 0.31$, $l_f = 2.01$, $w_g = 0.47$, $l_g = 1.77$, $w_h = 0.172$, $l_h = 8.61$, $w_i = 11.86$, and $l_i = 5.57$)

sharper passband-to-enlarged-stopband transitions—despite the higher design complexity of the method that exploits a fully heuristic/optimisation-based procedure. Finally, it should be noticed that the described design technique can also be applied to other classes of TFS, such as those which exhibit a band-stop-type behaviour so that the extension of their upper-passband bandwidth will be carried out as a future research work.

ACKNOWLEDGEMENT

This work was supported in part by the Spanish Ministry of Economy, Industry, and Competitiveness (State Research Agency) under Project TEC2017-82398-R and in part by the GOT ENERGY TALENT (GET) fellowship programme co-funded by the EU as part of the H2020-MSCA-COFUND programme (Grant Agreement number 754382).

REFERENCES

1. Gómez-García, R., Alonso, J.I.: Design of sharp-rejection and low-loss wide-band planar filters using signal-interference techniques. IEEE Microw Wireless Compon Lett. 15(8), 530–532 (2005)
2. Gómez-García, R., et al.: A class of microwave transversal signal-interference dual-passband planar filters. IEEE Microw Wireless Compon Lett. 19(3), 158–160 (2009)
3. Gómez-García, R., et al.: Wide-band signal-interference planar duplexer with contiguous single/dual-channel branches and its application to quasi-absorptive bandpass filters. IET Electron. Lett. 54(9), 578–580 (2018)
4. Gómez-García, R., et al.: Lossy flat-passband signal-interference microstrip filter. IET Electron. Lett. 55(4), 206–208 (2019)
5. Gómez-García, R.: High-rejection wideband signal-interference microstrip filters using rat-race couplers. IET Electron. Lett. 42(20), 1162–1163 (2006)
6. Sánchez-Soriano, M.-A., et al.: 'Reconfigurable-bandwidth bandpass filter within 10–50%'. IET Microw, Antennas Propag. 7(7), 502–509 (2013)
7. Sánchez-Soriano, M.-A., Bronchalo, E., Torregrosa-Penalva, G.: Compact UWB bandpass filter based on signal interference techniques. IEEE Microw Wireless Compon Lett. 19(11), 692–694 (2009)
8. Feng, W. J., Che, W. Q.: Ultra-wideband bandpass filter using broadband planar Marchand balun. IET Electron. Lett. 47(3), 198–199 (2011)
9. Ni, J., et al.: A compact bandpass filter based on right- and left-handed transmission line sections. IEEE Microw Wireless Compon Lett. 23(6), 279–281 (2013)
10. Mirzaee, M., Virdee, S.: UWB bandpass filter with notch-band based on transversal signal-interaction concepts. IET Electron. Lett. 49(6), 399–401 (2013)
11. Gómez-García, R., et al.: Hybrid-surface-acoustic-wave/microstrip signal-interference bandpass filters. IET Microw, Antennas Propag. 10(4), 426–434 (2016)
12. Mandal, M.K., Mondal, P.: Design of sharp-rejection, compact, wideband bandstop filters. IET Microw, Antennas Propag. 2(4), 389–393 (2008)
13. Sánchez-Soriano, M.-A., Torregrosa-Penalva, G., Bronchalo, E.: Compact wideband bandstop filter with four transmission zeros. IEEE Microw Wireless Compon Lett. 20(6), 313–315 (2010)
14. Gómez-García, R., et al.: Extended-stopband microstrip lowpass filter using rat-race directional couplers. IET Electron. Lett. 49(4), 272–274 (2013)
15. Loeches-Sánchez, R., et al.: Sharp-rejection highpass and dual-band bandpass planar filters with multi-transmission-zero-generation transversal cell. In: Proc. IEEE Radio Wireless Symp., pp. 147–149 (2015). San Diego, CA, USA
16. Muñoz-Ferreras, J.-M., Gómez-García, R.: A digital interpretation of frequency-periodic signal-interference microwave passive filters. IEEE Trans. Microw. Theory Techn. 62(11), 2633–2640 (2014)
17. Sánchez-Soriano, M.-A., Hong, J.-S.: Reconfigurable lowpass filter based on signal interference techniques. In: Proc. IEEE MTT-S Int. Microwave Symp., pp. 1–4 (2011). Baltimore, MD, USA
18. Gómez-García, R., Muñoz-Ferreras, J.-M., Sánchez-Renedo, M.: Signal-interference stepped-impedance-line microstrip filters and application to duplexers. IEEE Microw Wireless Compon Lett. 21(8), 421–423 (2011)
19. Sun, S., Zhu, L., Tan, H.H.: A compact wideband bandpass filter using transversal resonator and asymmetrical interdigital coupled lines. IEEE Microw Wireless Compon Lett. 18(3), 173–175 (2008)
20. Makimoto, M., Yamashita, S.: Microwave resonators and filters for wireless comminunications: Theory, design, and practice. Springer-Verlag Berlin Heidelberg New York (2001)
21. Chu, P., et al.: Wide stopband bandpass filter implemented by stepped impedance resonator and multiple in-resonator open stubs. IEEE Access. 7, 140631–140636 (2019)
22. Aouidad, M.H., et al.: Generic UHF bandpass filter with air-filled SIR coaxial resonators. In: Proc. Asia-pacific Microw. Conf., pp. 1486–1488 (2018). Kyoto, Japan
23. Morini, A., et al.: Systematic evaluation of spikes due to interference between cascaded filters. IEEE Trans. Microw. Theory Techn. 66(11), 4814–4819 (2018)

How to cite this article: Gómez-García R, Yang L, Muñoz-Ferreras JM. Optimisation-based design of transversal signal-interference microwave bandpass and lowpass filters with extended stopband. *IET Microw. Antennas Propag.* 2021;15:653–660. https://doi.org/10.1049/mia2.12091